Mechanism of CO Oxidation on Pt(111) in Alkaline Media

J. S. Spendelow, J. D. Goodpaster, P. J. A. Kenis, and A. Wieckowski*

Departments of Chemistry of Chemical & Biomolecular Engineering, University of Illinois at Urbana-Champaign, 600 South Mathews Avenue, Urbana, Illinois 61801

Received: January 5, 2006; In Final Form: March 8, 2006

Electrochemical techniques, coupled with in situ scanning tunneling microscopy, have been used to examine the mechanism of CO oxidation and the role of surface structure in promoting CO oxidation on well-ordered and disordered Pt(111) in aqueous NaOH solutions. Oxidation of CO occurs in two distinct potential regions: the prepeak (0.25−0.70 V) and the main peak (0.70 V and higher). The mechanism of reaction is Langmuir−Hinshelwood in both regions, but the OH adsorption site is different. In the prepeak, CO oxidation occurs through reaction with OH that is strongly adsorbed at defect sites. Adsorption of OH on defects at low potentials has been verified using charge displacement measurements. Not all CO can be oxidized in the prepeak, since the Pt−CO bond strength increases as the CO coverage decreases. Below $\theta_{CO} = 0.2$ monolayer, CO is too strongly bound to react with defect-bound OH. Oxidation of CO at low coverage occurs in the main peak through reaction with OH adsorbed on (111) terraces, where the Pt−OH bond is weaker than on defects. The enhanced oxidation of CO in alkaline media is attributed to the higher affinity of the Pt(111) surface for adsorption of OH at low potentials in alkaline media as compared with acidic media.

1. Introduction

Adsorption and oxidation of CO on Pt surfaces in aqueous electrolyte solutions has been extensively studied, primarily because of the importance of CO as a catalyst poison and also as a reaction intermediate on Pt and Pt/Ru catalysts in low-temperature direct methanol fuel cells (DMFCs) and reformate-fed hydrogen fuel cells.[1−11] Alkaline electrolytes have been shown to possess some advantages for CO oxidation on pure Pt catalysts, as the onset of CO oxidation on Pt occurs at lower relative potential in alkaline media than in acidic media.[10−15] Despite this advantage, most studies of CO and methanol oxidation have employed acidic electrolytes, since the problem of electrolyte carbonation in alkaline media complicates the use of alkaline electrolytes for fuel cells.[16] Fuel cells that incorporate electrolyte circulation provide the possibility of continuous removal of carbonates, suggesting that operation of an alkaline fuel cell under practical conditions is not impossible. In particular, a laminar flow fuel cell which lacks a membrane to separate the anodic and cathodic compartments[17−21] shows promise as a fuel-flexible, electrolyte-flexible system in which electrolyte repurification can be incorporated and clogging of membrane pores with carbonates cannot occur.

A detailed understanding of the mechanism of CO oxidation on Pt surfaces would be useful in optimizing Pt-based catalysts for fuel cell reactions. In general, Langmuir−Hinshelwood (L−H) mechanisms are favored for most surface reactions occurring at the solid−gas interface, but the situation is different at the solid−liquid interface. The principal reason for the scarcity of Eley−Rideal (E−R) mechanisms at the solid−gas interface is the relatively low frequency of collisions between adsorbed and nonadsorbed species, as compared with the frequency of collisions between two adsorbed species or an adsorbed species and a trapped species.[22] This difference becomes particularly pronounced when the partial pressure of at least one of the reactants becomes very low. At the solid−liquid interface, the orders-of-magnitude greater density of a liquid as compared with a gas causes an orders-of-magnitude greater frequency of collisions between adsorbed and nonadsorbed species, so E−R reactions should be much more common at solid−liquid interfaces than at solid−gas interfaces.

Nevertheless, in acidic electrolytes, CO oxidation is known to occur through an L−H mechanism in which the adsorbed CO reacts with an adsorbed oxygen-containing species derived from water.[1−7] Competition between CO and OH for adsorption sites is evinced by the peaked current transient during potentiostatic oxidation of a saturated CO adlayer. Initiation of the reaction through an E−R mechanism prior to the onset of L−H oxidation has been proposed,[3] but most authors favor an L−H mechanism for CO oxidation even during the nucleation phase.[5−7] In alkaline electrolytes, some authors have asserted an L−H mechanism,[10,13] while others have proposed an E−R mechanism.[23] Our previous study[11] found some evidence to support an E−R reaction at low potential, but we were not able to eliminate the possibility of an L−H reaction in which CO and OH adsorption is noncompetitive. In contrast to the acidic case, potentiostatic CO oxidation at low potential in an alkaline electrolyte produces a monotonically decaying current transient. The lack of a peaked profile means that the activity of the oxidant species does not significantly increase as the CO coverage decreases, indicating that the oxidant cannot be a species that competes with CO for adsorption sites. Rather, the oxidant must be a nonadsorbed OH^- (E−R mechanism) or an adsorbed oxygen-containing species that does not compete with CO for the same adsorption sites (noncompetitive L−H mechanism).

The results reported here indicate that a noncompetitive L−H mechanism involving OH bound on defects is the operative mechanism at low potentials ($E < 0.65$ V), with a competitive L−H mechanism involving OH bound on terraces occurring at

* To whom correspondence should be addressed. Phone: (217) 333-7943. Fax: (217) 244-8068. E-mail: andrzej@scs.uiuc.edu.

10.1021/jp060100c CCC: $33.50
Published on Web 04/22/2006

higher potential. This conclusion is upheld by analysis of the Tafel slope, the reaction order in OH^-, the effect of the surface structure, and the effect of the adsorption environment on the rate of CO oxidation at low potentials.

2. Experimental Section

2.1. Electrochemical Experiments. A 2 mm bead-type Pt(111) electrode was employed in the electrochemical experiments. Materials used were Ar and H_2 (SJ Smith, ultrahigh purity), CO (SJ Smith, research grade), H_2SO_4 and $HClO_4$ (GFS, doubly distilled from Vycor), and NaOH and NaF (Merck, Suprapur). Electrochemical measurements were performed in a two-compartment cell with a Pt wire counter electrode and a Ag/AgCl reference electrode (BAS, $[Cl^-] = 3$ M), although all potentials are quoted on the RHE scale unless otherwise indicated. An Autolab PGSTAT 30 potentiostat was used for all measurements. Prior to measurements, the clean electrode was annealed in a H_2 flame for several seconds and cooled in a H_2 + Ar stream. The electrode was transferred to the electrochemical cell with a drop of H_2-saturated Millipore water to protect against oxidation and contamination of the working surface. After potential cycling in 0.1 M H_2SO_4 to confirm the surface quality and cleanliness, the electrode was rinsed with Ar-purged water, and the H_2SO_4 solution was drained and replaced with 0.1 M NaOH solution under a continuous Ar blanket at open circuit potential. Adsorption of CO was performed by replacing the Ar blanketing gas with a 5% CO/95% Ar stream while the electrode was maintained in meniscus configuration at a potential of 0.10 V. Adsorption of CO in meniscus configuration allows measurement of the current transient resulting from displacement of adsorbed species (the CO charge displacement technique[24]). Integration of the current transient provides a measurement of the surface charge associated with specific adsorption at the potential at which the charge displacement is performed. The surface charge density associated with adsorption may be calculated at any other potential by integration of the background CV. After CO adsorption was completed (approximated as 30 s after the completion of the desorption current transient, typically about 90 s of CO exposure total), the electrode was raised from solution and the cell was purged with Ar for 60 s, which was sufficient to remove all traces of CO. Emersion of the electrode during Ar purging limited surface contamination, which otherwise may occur due to the high rate of mass transfer created by solution purging. This procedure yielded a saturated CO adlayer (0.69 monolayer (ML) in CO-free solution), as determined by integration of the CO oxidation current. Subsaturated CO adlayers were produced by bubbling Ar gas through the solution, with the electrode immersed, and injecting a small amount of CO (0.05−1.0 mL) into the Ar stream using a gastight syringe. The electrode was raised from the solution after 20 s of bubbling, and the solution was purged with pure Ar for an additional 60 s to remove all traces of CO.

2.2. STM Experiments. Scanning tunneling microscopy (STM) was performed in situ in 0.1 M NaOH solution using a Molecular Imaging Pico STM instrument. A 1 cm cylindrical Pt(111) crystal was used for STM. After flame annealing, cooling in Ar + H_2, and dipping in water, the crystal was protected by adsorption of iodine from 1 mM KI solution and transferred to the STM cell, where the iodine was removed by holding the potential at approximately 0.1 V while rinsing with 0.1 M NaOH. Imaging was performed in constant current mode with a tunneling current of 1−2 nA. Electrochemically etched tungsten tips, coated with paraffin wax, were used for all STM measurements. The reference electrode was a Ag/AgCl electrode connected to the cell by an electrolyte bridge filled with 0.1 M NaOH.

2.3. Surface Cleanliness. The preparation (and maintenance) of clean Pt(111) surfaces requires special attention in alkaline solutions, which tend to be more susceptible to contamination than comparable solutions of H_2SO_4 or $HClO_4$. In particular, previous studies have shown a voltammetric peak corresponding to reduction of an adsorbed species at 0.54 V, which was identified as an iron-containing adsorbate by analysis of X-ray photoelectron spectra.[25] In most cases, the Fe contamination can be avoided through use of the highest quality grade of NaOH. In experiments using CO, further care must be taken to ensure that volatile iron carbonyl species are not present, either through use of Al cylinders for CO storage or by removing Fe from contaminated CO gas. Removal of Fe can be accomplished by thoroughly contacting the CO with solid or aqueous NaOH.[26] For experiments that require either an extremely long duration or high mass transfer of solution-phase species to the electrode surface, significant Fe contamination can develop even when using the highest purity chemicals. In this situation, adding a large surface area of Fe-free Pt (black Pt wire) to the electrochemical cell greatly reduces the severity of Fe contamination, as most Fe is removed from solution by adsorption onto the Pt wire surface. Using this method, a contaminated Pt(111) surface can even be cleaned, as Fe slowly desorbs from the Pt(111) and adsorbs on the Pt wire. The adsorbed Fe can be periodically removed from the Pt wire by immersion in acidic solutions. Use of the above procedures in the present study has eliminated most Fe contamination.

Other unknown contaminants may appear under some circumstances, resulting in poor-quality background cyclic voltammograms. In general, these contaminants can be eliminated by avoiding exposure of the Pt(111) surface to laboratory air. Some exposure to air is unavoidable during the flame annealing and transfer process, but in this study the resulting contaminants were readily removed by performing cyclic voltammetry between 0.05 and 0.85 V in 0.1 M H_2SO_4 solution. After this cleaning step, the H_2SO_4 solution was drained from the cell, the crystal was rinsed with a jet of Ar-saturated water, and the cell was filled with 0.1 M NaOH solution, all performed under a blanket of Ar to avoid any exposure to laboratory air. This procedure consistently prevented any detectable contamination.

3. Results and Discussion

3.1. Pt(111) Surface: Structure and Voltammetry. Figure 1A shows a background cyclic voltammogram (CV) for Pt(111) in 0.1 M NaOH. To a first-order approximation, the pseudocapacitance at potentials less positive than 0.40 V can be assigned solely to adsorption of H, while between 0.65 and 0.85 V OH adsorption occurs.[27−29] In the intermediate "double-layer" region, 0.40−0.65 V, the surface is free of adsorbed H and OH. A good understanding of the surface electrocatalytic properties, however, requires a more nuanced description. Specifically, the above interpretation would be correct for an ideal (111)-oriented surface, but even the most carefully prepared (111) surface contains a finite defect density, which in some cases can dominate the electrocatalytic behavior.[30] This is the case even on the state-of-the-art surfaces employed in this study (Figure 1).

Very small errors in orientation and cutting produce a low level of (110) and (100) steps on the otherwise well-ordered Pt(111) surface, producing adsorption peaks at 0.27 and 0.40 V, respectively.[28] These features are barely observable on a well-

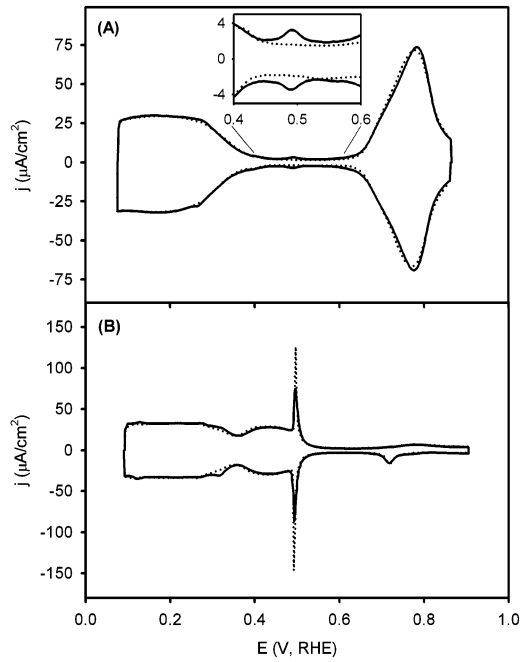

Figure 1. Pt(111) cyclic voltammograms in 0.1 M NaOH (A) and 0.1 M H_2SO_4 (B), scan rate 50 mV/s. Dotted line: freshly annealed surface. Solid line: same surface after six scans up to 1.25 V in 0.1 M NaOH.

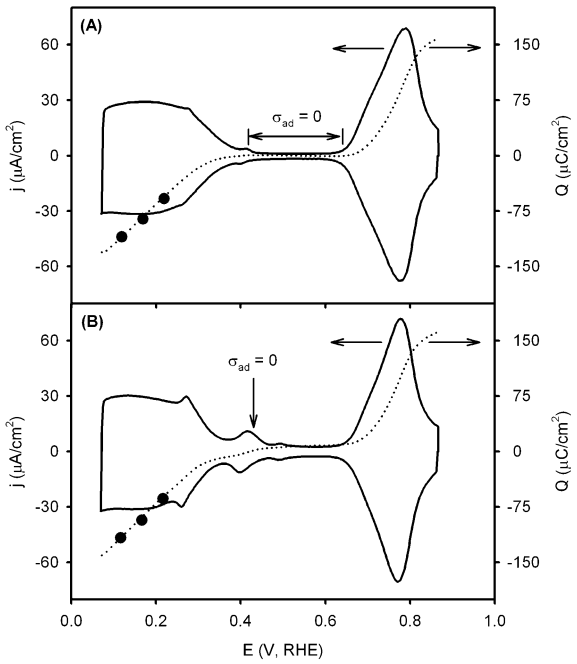

Figure 2. Results of CO charge displacement experiments on well-ordered (A) and disordered (B) Pt(111) surfaces in 0.1 M NaOH. The surface in (B) was disordered by 10 scans up to 1.31 V in 0.1 M NaOH. Solid line: background cyclic voltammogram. Dotted line: charge density of adsorbed species. Charge displacement was performed at 0.12, 0.17, and 0.22 V (black circles).

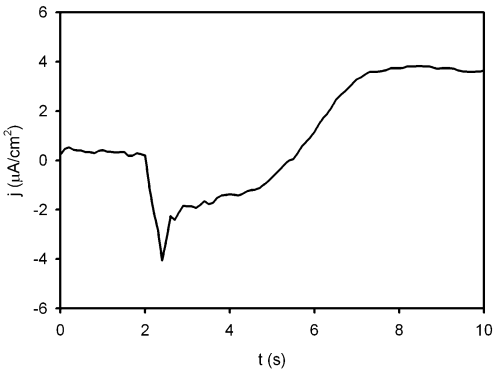

Figure 3. Charge displacement on a disordered Pt(111) surface at 0.42 V in 0.1 M NaOH. CO was introduced into the cell at $t = 2$ s.

ordered surface such as the one represented by Figure 1A, but may still play a role in CO oxidation due to the high mobility of CO on Pt surfaces.[31] The adsorbate at these potentials has been assigned to underpotentially deposited (upd) H by most authors, although the concurrent existence of adsorbed OH at these defects has also been proposed by some.[10] Recent semiempirical calculations predict that OH adsorption on Pt in alkaline solutions should commence at 0.61 V, which is in good agreement with the observed onset potential of 0.65 V for OH adsorption on terraces.[32] Nevertheless, OH adsorption at defect sites occurs at lower potentials than on terraces, as confirmed recently on Pt nanoparticles,[33] since the Pt−OH bond is stronger on defect sites than on terraces.[34] Charge displacement experiments confirm the existence of adsorbed OH in this region (Figure 2). The surface charge density resulting from adsorbed species (σ_{ad}) at 0.12 V was determined by measuring the displaced charge upon exposure to CO, and σ_{ad} at all other potentials was obtained by integration of the background CV starting from 0.12 V. In our notation, σ_{ad} represents the charge on the metal side of the interface, so a positive value of σ_{ad} indicates net anion adsorption, while a negative value corresponds to net adsorption of cations (upd H). Charge displacement was also performed at 0.17 and 0.22 V, and the good agreement between the measured values and the integrated charge density demonstrates the accuracy of this method.

As an aside, we note that the charge displacement method has been used to estimate the potential of zero total charge (pztc) of various metal surfaces.[24,35] The potential at which $\sigma_{ad} = 0$ is an approximation of the pztc, although for a more accurate estimation the free charge associated with nonspecifically adsorbed charged species must also be taken into account. This is the subject of a parallel investigation in our laboratory.[36]

On well-ordered surfaces (Figure 2A) the OH coverage is too low to observe by the charge displacement method, such that $\sigma_{ad} \approx 0$ throughout the double-layer region (0.40−0.65 V). Introduction of defects reveals the presence of OH, as $\sigma_{ad} > 0$ throughout the double-layer region for a disordered surface (Figure 2B). Unfortunately, at potentials higher than 0.25 V the incipient oxidation of CO skews charge displacement measurements, necessitating the integration of the background CV from potentials lower than 0.25 V to ascertain σ_{ad} in this region. Qualitative information can still be obtained by performing charge displacement at higher potentials. Adsorption of CO at 0.42 V (Figure 3) results in a brief negative-going current transient (prior to the onset of CO oxidation), which can be attributed to desorption of OH from defect sites. The charge displacement experiments depicted in Figures 2 and 3 demonstrate that OH adsorption occurs at low potentials, with OH localized at defect sites, and that some overlap occurs between the potential range for H adsorption and the potential range for OH adsorption. This interpretation is in agreement with the observation that O adsorption is stronger at step and kink sites than on terrace sites on vicinal Pt(111) surfaces in an ultrahigh vacuum (UHV),[37−41] as well as the recent in situ observation of OH adsorption on edge sites at lower potential than on terraces.[33]

In the region between 0.40 and 0.65 V, no detectable specific adsorption of charged species occurs on well-ordered surfaces,

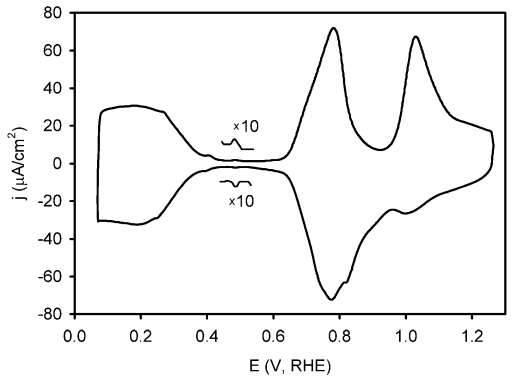

Figure 4. Cycling up to 1.25 V results in the adsorption of O at potentials higher than 0.85 V, and the development of a reversible peak at 0.49 V. The third scan up to 1.25 V at 50 mV/s is shown.

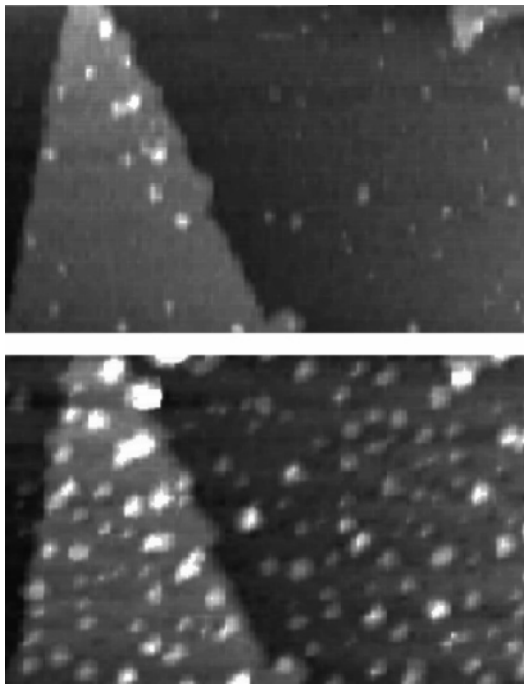

Figure 5. Pt(111) surface imaged by in situ STM in 0.1 M NaOH ($E_{tip} = 0.4$ V, $E_{surface} = 0.5$ V). The top and bottom images show the same 40 × 80 nm area of the surface. Top: the surface had been scanned up to 1.35 V three times. Bottom: the surface had subsequently been scanned up to 1.40 V three times and 1.45 V three times, creating Pt islands (1−4 nm diameter, monatomic height).

but on lightly disordered surfaces an adsorption peak becomes visible at 0.49 V (inset to Figure 1A). This feature is also visible in earlier published CVs,[42,43] but has not previously been interpreted. Cycling the potential up to 1.25 V (Figure 4) causes this peak to appear. The adsorption and desorption of O at potentials higher than 0.90 V results in a mild surface disordering, causing rapid growth of the 0.49 V peak, although features associated with (110) and (100) steps increase only slightly. The 0.49 V peak can also be developed to a small extent through repeated cycles of CO adsorption and stripping.

Electrochemical scanning tunneling microscopy is an ideal technique to examine the changes in surface structure resulting from potential cycling into the irreversible oxidation region (potentials higher than 0.90 V). Figure 5 shows the effect of scanning to relatively high potentials. Scanning up to 1.35 V, and subsequently to 1.40 and 1.45 V, results in the formation of Pt islands with diameters ranging from 1 to 4 nm. The edges of these islands are characterized by steps with (110) and (100)

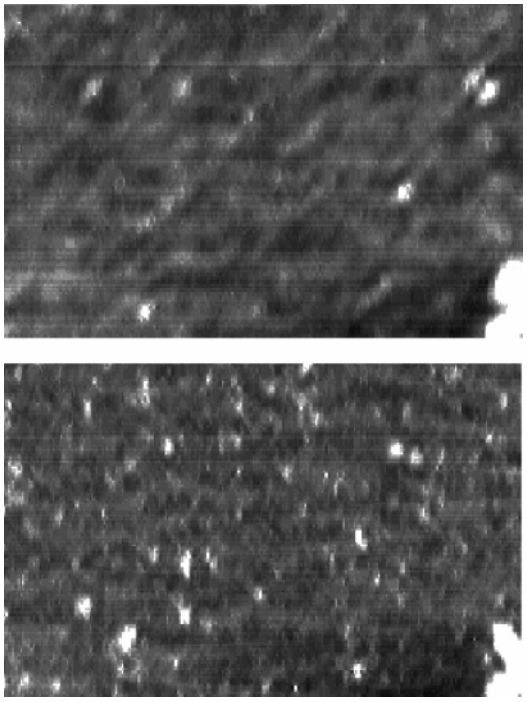

Figure 6. Pt(111) surface imaged by in situ STM in 0.1 M NaOH ($E_{tip} = 0.4$ V, $E_{surface} = 0.5$ V). The top and bottom images show the same 20 × 40 nm area of the surface. Top: freshly annealed surface. Bottom: after cycling up to 1.20 V 12 times.

geometry, as demonstrated in the background CV for a similar surface (Figure 2B). In contrast, potential cycling with a less positive anodic potential limit (1.25 V or lower) does not result in a significant increase in the population of 1−4 nm islands, instead producing smaller islands (diameter <1 nm), as shown in Figure 6. These islands are the source of the voltammetric peak at 0.49 V in 0.1 M NaOH.

A surface with a well-developed peak at 0.49 V in alkaline solutions can be transferred to acidic solutions for further characterization. As illustrated in Figure 1B, the structural feature that causes the 0.49 V peak in alkaline solutions also gives rise to a voltammetric peak at 0.32 V in sulfuric acid solution. Studies on vicinal Pt(111) surfaces have shown that this peak is related to H adsorption at kink sites.[44,45] These kink sites are characterized by Pt atoms with a lower coordination number than Pt atoms in (110) or (100) steps, and have the same geometry as sites on the edge of very small Pt islands (Figure 7). This voltammetric evidence therefore supports the assignment of the 0.49 V peak in 0.1 M NaOH to an adsorption event occurring at very small Pt islands. For the remainder of the discussion, surfaces that have a high density of large islands, characterized by (110) and (100) steps sites, will be referred to as "highly disordered," while surfaces with a high density of small islands but few large islands will be referred to as "lightly disordered".

Since voltammetric studies in which other alkali-metal cations (Li^+, Cs^+) are substituted for Na^+ produce no change in the CV at potentials below 0.60 V, the participation of the alkali-metal cation in the adsorption peak at 0.49 V can be excluded. Therefore, the peak at 0.49 V must correspond to either H or OH adsorption, or a combination of the two. The behavior of the peak at 0.49 V in the presence of other adsorbates further clarifies the nature of the adsorption event occurring in this peak. A significant shift in the peak potential occurs when adsorbed CO is present at subsaturated levels. Increasing the CO coverage in the range from 0 to 0.17 ML results in a linear increase in

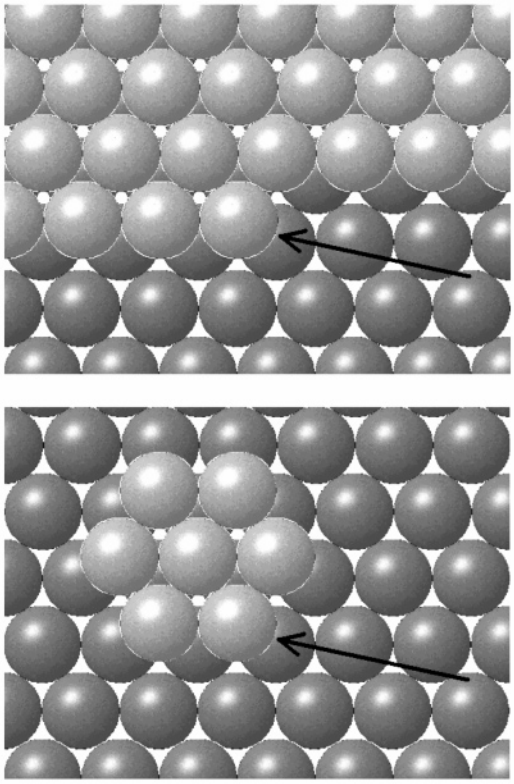

Figure 7. A kink site, as indicated by the arrow in the top diagram, has the same local geometry as a site on the edge of the small island (diameter 0.8 nm) shown in the bottom diagram.

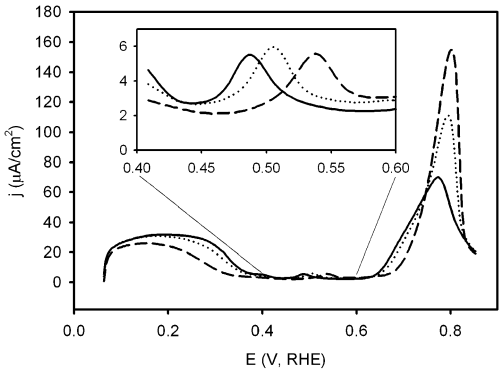

Figure 8. First positive-going scan on a lightly disordered Pt(111) surface with a subsaturated CO adlayer in 0.01 M NaOH. Solid line: 0 ML CO. Dotted line: 0.07 ML CO. Dashed line: 0.17 ML CO. Scan rate 50 mV/s.

the peak potential from 0.49 to 0.54 V, without any change in the shape or size (Figure 8). We also observed a similar shift with adsorbed iodine. Both H and OH are expected to interact repulsively with CO and I,[46−48] so the H or OH binding energy should decrease with increasing coverage of CO or I. For OH, a positive peak shift implies a weaker binding energy, whereas for H, a positive peak shift corresponds to a stronger binding energy. Therefore, the positive peak shift with adsorbed CO or I indicates that the adsorbate in the 0.49 V peak is at least partly OH.

3.2. CO Oxidation. A Pt(111) surface that has been disordered such that it shows a voltammetric peak at 0.49 V has electrocatalytic properties for CO oxidation that are strikingly different from those of a well-ordered Pt(111) surface (Figure 9). For both types of surfaces, CO oxidation may be divided into a prepeak region (less positive than 0.70 V) and a

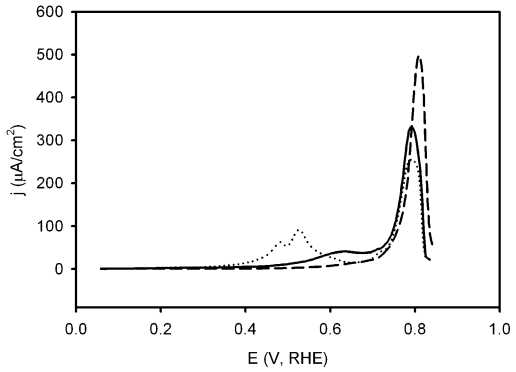

Figure 9. Oxidation of preadsorbed CO on Pt(111) in 0.1 M NaOH solution. Solid line: well-ordered Pt(111). Dotted line: lightly disordered Pt(111). Dashed line: well-ordered Pt(111) on which CO was adsorbed in 0.1 M H_2SO_4 solution, followed by transfer to 0.1 M NaOH. Scan rate 50 mV/s.

main peak region (more positive than 0.70 V). Prepeak, in this sense, refers only to the potential region, and not to the shape of the current−potential plot, which may show one or more peaks or only a small wave depending on the surface ordering and the method of CO adsorption. For instance, lightly disordering the Pt(111) surface causes a sharp peak to appear in the prepeak region. It also causes a net transfer of CO stripping charge from the main peak region to the prepeak, although in both cases the total CO stripping charge (corrected for OH readsorption) is the same, $330 \pm 10\ \mu C/cm^2$, corresponding to a CO coverage of approximately 0.69 ML. The third trace in Figure 9, which shows the case where CO is adsorbed in 0.1 M H_2SO_4 and transferred to 0.1 M NaOH, is discussed in section 3.2.3.

3.2.1. CO Oxidation: Main Peak. Oxidation of CO in the main peak region was assigned to an L−H mechanism (eqs 1 and 2)

$$CO_{ad} + OH_{ad} \rightarrow COOH_{ad} \quad (1)$$

$$COOH_{ad} + OH_{ad} \rightarrow CO_2 + H_2O \quad (2)$$

in our previous study,[11] and this interpretation is further supported by the results of this study. In alkaline electrolytes, the product CO_2 is rapidly converted to CO_3^{2-} by reaction with OH^-. In the main peak region, OH adsorbed on terraces acts as the oxidant, as inferred from the position of the main CO stripping peak within the OH adsorption region and the inability of OH adsorbed at defects to react with CO at low CO coverage. Since OH and CO compete for adsorption sites on terraces, potentiostatic oxidation of a saturated CO adlayer would be expected to produce a peaked current−time profile, as commonly observed in acidic media.[1,5,8,49] This expectation is not realized during oxidation of CO adsorbed in 0.1 M NaOH,[11] however, as a result of the oxidation of prepeak CO *prior* to the onset of main peak CO oxidation. Since potentiostatic oxidation of prepeak CO produces a monotonically decaying current transient,[11] and since roughly half of the CO is oxidized in the prepeak, by the time main peak CO oxidation commences the CO coverage is already so low that the current transient looks like a simple decay; essentially, only the decaying side of the peak is observable. This interpretation was confirmed by oxidizing only the prepeak (by voltammetry) in alkaline media, followed by transfer to 0.1 M $HClO_4$. Potentiostatic oxidation of the remaining CO in the acid solution produced a monotonically decaying current transient (Figure 10), indicating that, indeed, the CO coverage after oxidation of the prepeak in

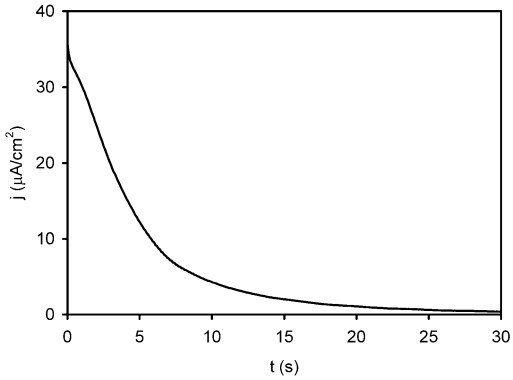

Figure 10. Potentiostatic oxidation at 0.64 V of a subsaturated CO adlayer on Pt(111) in 0.1 M $HClO_4$. The adlayer was prepared by adsorbing CO in 0.1 M NaOH and scanning once up to 0.67 V to oxidize the prepeak, followed by transfer to $HClO_4$.

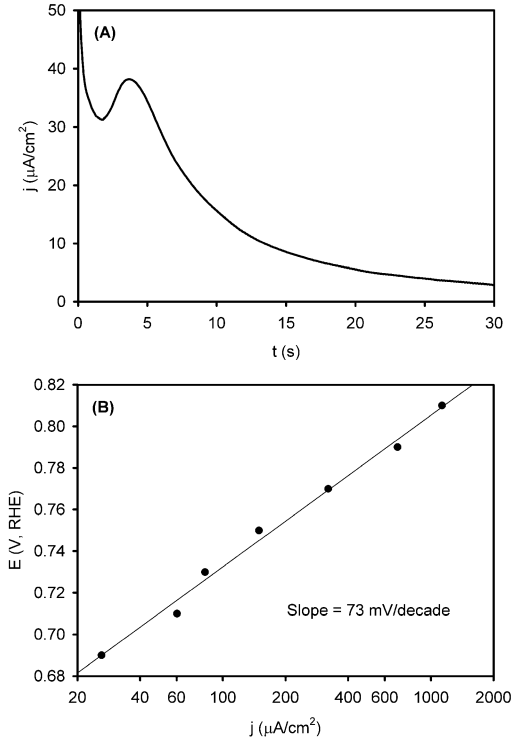

Figure 11. (A) Oxidation of preadsorbed CO on a well-ordered Pt-(111) surface at 0.73 V in 0.1 M NaOH. CO was first adsorbed to saturation coverage in 0.1 M H_2SO_4, followed by transfer to CO-free 0.1 M NaOH solution, and the potential was stepped from 0.10 to 0.73 V. (B) Tafel slope for oxidation of a subsaturated CO adlayer in the main peak region.

alkaline solutions is too low for a peak to occur during main peak potentiostatic CO oxidation, whether it is performed in alkaline or acidic media. Decreasing the size of the prepeak allows the competitive nature of the CO and OH coadsorption to become more visible. Adsorption of CO in 0.1 M H_2SO_4 and subsequent transfer to 0.1 M NaOH results in a decrease of the size of the prepeak (further discussed in section 3.2.3), coupled with a positive shift in the potential of the prepeak so that it overlaps with the main peak (dashed line in Figure 9). Oxidation of a CO adlayer prepared in this way reveals the peaked current−time profile of the potentiostatic main peak CO oxidation (Figure 11A). This peaked profile confirms the L−H oxidation of CO, with competitive adsorption of CO and OH, in the main peak region.

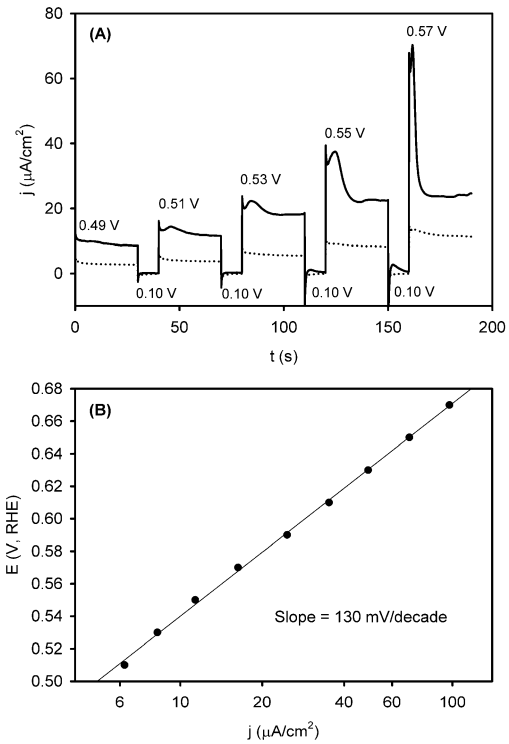

Figure 12. (A) Oxidation of dissolved CO on Pt(111) surfaces in 0.01 M NaOH solution saturated with 5% CO/95% Ar. Solid line: disordered Pt(111). Dotted line: well-ordered Pt(111). (B) Tafel slope for oxidation of bulk CO in the prepeak region.

Analysis of the Tafel slope of the initial current after a step from 0.10 V to the final potential (ranging from 0.69 to 0.81 V) also supports the L−H reaction between adsorbed CO and OH on terraces (Figure 11B). Subsaturated adlayers, prepared from saturated adlayers by a single potential scan up to 0.70 V, were used for the Tafel analysis to reduce the overlapping current from oxidation of prepeak CO. The Tafel slope measured by this technique in the main peak region is 73 mV per decade, very similar to previously published Tafel slopes for CO oxidation on Pt(111) in sulfuric acid electrolyte.[3,5,50,51] This value is in reasonably good agreement with the theoretical value of 60 mV per decade for L−H CO oxidation.

3.2.2. CO Oxidation: Prepeak. In our earlier report,[11] we interpreted the monotonically decaying current transient during oxidation of a saturated CO adlayer on well-ordered Pt(111) surfaces as an indication of either an L−H mechanism in which CO and OH do not compete for adsorption sites or E−R mechanism (eq 3). The subsequent oxidation of adsorbed COOH

$$CO_{ad} + OH^- \rightarrow COOH_{ad} + e^- \qquad (3)$$

could be either E−R (eq 4) or L−H (eq 2). The shape of the CO oxidation current transient, shown for bulk CO oxidation

$$COOH_{ad} + OH^- \rightarrow CO_2 + H_2O + e^- \qquad (4)$$

in Figure 12, reflects the rate-limiting step in CO oxidation, which in acidic electrolytes is widely believed to be the reaction between CO and an adsorbed oxygen-containing species. For a well-ordered Pt(111) surface, the monotonic decay displayed in Figure 12 is consistent with the E−R mechanism and with the results of our previous study,[11] but on a disordered surface, a peak appears in the current transient under certain conditions. This peak is only manifested at very high CO coverage, requiring the presence of dissolved CO in solution during CO

oxidation. Also, the peak only appears at potentials more positive than 0.49 V. Experiments that fail to meet both these criteria yield a monotonically decaying current transient similar to the current transient on a well-ordered surface (though with higher current density). Several conclusions can be drawn from these data. The appearance of a peak in the CO oxidation current transient on a disordered surface demonstrates the L−H oxidation of CO by OH adsorbed at defect sites in the prepeak region. The lack of a peak at even slightly subsaturated CO coverage reveals that the oxidant OH species is a strong competitor with CO for adsorption at defect sites. It is only at the highest CO coverage that the CO can begin to outcompete OH for these defect sites, and apparently even on a fully CO saturated surface some OH is always formed at defect sites, explaining the high currents visible at the onset of potentiostatic CO stripping in Figure 12. Thus, we find the experimental results to be consistent with an L−H mechanism in which OH is successful at outcompeting CO for adsorption at defect sites, except at the highest CO coverages, while CO occupies all terrace sites.

The onset of the peak in the CO oxidation current transient at potentials more positive than 0.49 V demonstrates the nucleation of OH at defects in this potential range. Since the peak is absent at lower potentials, this particular OH species seems not to exist below 0.49 V, so that the current at less positive potential must be attributed to the existence of OH adsorbed at different kinds of defects. This result is not surprising when consideration is given to the heterogeneous nature of the disordered surface.

Although the appearance of a peak in the CO oxidation current transient under certain conditions confirms the existence of an L−H mechanism for CO oxidation on a disordered Pt(111) surface, the results are less definitive on a well-ordered Pt(111) surface. Still, the demonstration of a quasi-monotonically decaying current transient for the L−H reaction on a disordered surface suggests that the monotonic decay visible in the current transient for a well-ordered surface (Figure 12) is compatible with either noncompetitive L−H or E−R kinetics, given that even the highest quality "well-ordered" surface has a finite defect density.

Analysis of the initial current in experiments similar to those shown in Figure 12A yields a Tafel slope of 130 mV per decade for a well-ordered Pt(111) surface in the presence of dissolved CO (Figure 12B). If the rate-limiting step in CO oxidation were the E−R reaction between CO and OH^-, the Tafel slope would be expected to be 60/α mV per decade, where α is the transfer coefficient; typically, $0.3 < \alpha < 0.7$.[52] Therefore, the Tafel slope should be between 90 and 200 mV if the mechanism is E−R. Although the measured Tafel slope does not rule out an E−R mechanism, a comparison of the Tafel slope and the reaction order in OH^- reveals inconsistencies that argue against an E−R mechanism. Since the CO oxidation current (j) at constant CO coverage is a function of the electrode potential and the concentration of OH^- ions in solution, the triple product rule gives the relationship

$$\left(\frac{\partial[\log(j)]}{\partial[\log(C_{OH^-})]}\right)_E = -\left(\frac{\partial[\log(j)]}{\partial E}\right)_{C_{OH^-}}\left(\frac{\partial E}{\partial[\log(C_{OH^-})]}\right)_j \quad (5)$$

The left side of eq 5 represents the reaction order in OH^-, while the right side is the product of the inverse of the Tafel slope and the shift of the CO stripping voltammogram with potential on a pH-independent potential scale. This last term can be evaluated from the pH-dependent CO stripping data shown in

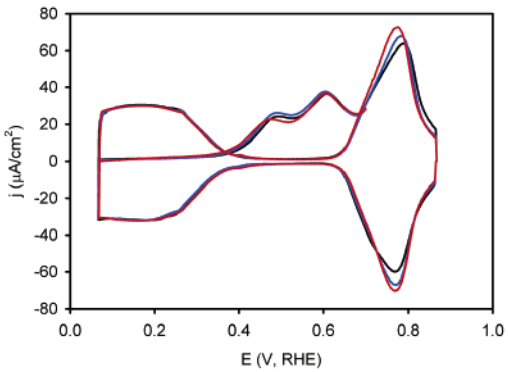

Figure 13. Effect of OH^- concentration on oxidation of adsorbed CO on a well-ordered Pt(111) surface. Each voltammogram was collected using the same Pt(111) surface. Black line: CO stripping in 0.001 M NaOH + 0.1 M NaF. Blue line: CO stripping in 0.01 M NaOH + 0.09 M NaF. Red line: CO stripping in 0.1 M NaOH. Background CVs are superimposed.

Figure 13. This figure demonstrates that, when plotted on the pH-relative RHE potential scale, the CO stripping prepeak is virtually the same over a pH range of at least 11−13 when the double-layer structure is kept constant through a 1:1 substitution of F^- for OH^- ions. Therefore, on a pH-independent scale such as the SHE scale, the potential must shift by −60 mV for every decade increase in OH^- concentration to keep the same CO oxidation current. Thus, eq 5 reduces to

$$\left(\frac{\partial[\log(j)]}{\partial[\log(C_{OH^-})]}\right)_E = -\left(\frac{1}{130}\frac{\text{decade}}{\text{mV}}\right)\left(-60\frac{\text{mV}}{\text{decade}}\right) = 0.46 \quad (6)$$

The roughly half-order dependence on OH^- concentration, which is the same dependence found by Tripkovic et al. for methanol oxidation on Pt(111) in alkaline media,[29] is inconsistent with an Eley−Rideal rate-limiting step, which should show a first-order dependence on OH^-.

Both the Tafel slope and the reaction order are consistent with an L−H mechanism in which the OH coverage is described by a mean field Frumkin isotherm (eq 7). The parameter r in

$$\frac{\theta_{OH}}{1-\theta_{OH}} = KC_{OH^-}\exp\left(\frac{EF - r\theta_{OH}}{RT}\right) \quad (7)$$

eq 7 represents the effect of adsorbate−adsorbate interactions, which are known to be repulsive for OH,[53] so that the sign of r is positive. For such an isotherm, the OH coverage, when between 20% and 80% of the saturation value, may be approximated as

$$\theta_{OH} = \frac{RT}{r}\ln(KC_{OH^-}) + \frac{EF}{r} \quad (8)$$

The rate constant for the reaction between CO and OH can also be described with a Frumkin term (represented by the parameter g) to account for the effect of OH−OH, OH−CO, and OH−COOH interactions on the activation barrier:

$$k = k_0\exp(g\theta_{OH}/RT) \quad (9)$$

By combining eqs 8 and 9, the CO oxidation current may be written as

$$j = k\theta_{OH}\theta_{CO} = k_0\exp\left(\frac{g}{r}\left(\ln(KC_{OH^-}) + \frac{EF}{RT}\right)\right)\left(\frac{RT}{r}\ln(KC_{OH^-}) + \frac{EF}{r}\right)\theta_{CO} \quad (10)$$

The expected reaction order (eq 11) and Tafel slope (eq 12) can be calculated directly from eq 10.

$$\frac{\partial[\log(j)]}{\partial[\log(C_{OH^-})]} = \frac{g}{r} + \frac{RT}{r\theta_{OH}} \tag{11}$$

$$\frac{\partial E}{\partial[\log(j)]} = \left(\frac{2.303RT}{F}\right)\Big/\left(\frac{g}{r} + \frac{RT}{r\theta_{OH}}\right) \tag{12}$$

The value of RT/r has been estimated at roughly 0.5 for OH adsorption on Pt(111) terraces in NaOH solutions.[53] This relatively weak repulsion explains why the Tafel slope for CO oxidation by OH on terraces (73 mV per decade) is relatively close to the theoretical value of 60 mV per decade, which assumes that OH coverage can be described by the Nernst equation and that the reaction rate constant does not depend on the coverage; i.e., site saturation and adsorbate−adsorbate interactions are negligible. The much higher Tafel slope during CO oxidation in the prepeak indicates a larger role of adsorbate−adsorbate repulsions, which could result from OH adsorption on defects rather than on terraces. In particular, the electronic perturbations caused by the stronger metal−adsorbate bonds at defects should lead to stronger through-metal repulsions. Also, we note that other metal surfaces in alkaline media have been reported to have values of RT/r of less than 0.1 for OH adsorption.[54,55] As a first approximation, the term $RT/(r\theta_{OH})$ can be neglected, so that eqs 11 and 12 can be rewritten as

$$\frac{\partial[\log(j)]}{\partial[\log(C_{OH^-})]} = \frac{g}{r} \tag{13}$$

$$\frac{\partial E}{\partial[\log(j)]} = 60\frac{r}{g} \tag{14}$$

Assuming that OH−OH repulsions are the primary cause of the OH-coverage-dependent perturbations in the free energy of reaction for eq 1 (i.e., they are more significant than OH−CO and OH−COOH interactions), the parameter r can be taken as approximating the dependence of the free energy of reaction on the coverage of OH. With this approximation, the quantity g/r reduces to the transfer coefficient, α, which typically has a value close to 0.5. Therefore, substituting this value of g/r into eqs 13 and 14 yields an expected reaction order in OH^- of 0.5 and an expected Tafel slope of 120 mV per decade, in good agreement with the experimentally measured reaction order of 0.46 and Tafel slope of 130 mV per decade. Of course, a number of assumptions were made in the above analysis. These assumptions can be tested by using the Frumkin isotherm in its exact form (eq 7). Replacing the approximate Frumkin isotherm in eq 10 with the exact form yields

$$j = k_0 \exp\left(\frac{gKC_{OH^-}(1-\theta_{OH})}{RT}\exp\left(\frac{EF - r\theta_{OH}}{RT}\right)\right) \times \left(KC_{OH^-}(1-\theta_{OH})\exp\left(\frac{EF - r\theta_{OH}}{RT}\right)\right)\theta_{CO} \tag{15}$$

The derivation of eq 15 does not include any approximations of the Frumkin isotherm or assumptions about the relative values of the parameters. Although use of the exact form of the Frumkin isotherm (eq 7) does not allow an analytical solution of θ_{OH} as a function of potential, and thus does not allow analytical calculation of the Tafel slope, the predictions of eq 15 can still be compared with experimental observations to verify the applicability of the model. The red trace in Figure 14 represents a simulated CO bulk oxidation experiment ($\theta_{CO} = 0.75$, $C_{OH^-} = 0.1$ M) in which the current−potential relationship was calculated from eq 15, with θ_{OH} calculated from eq 7 using the Newton−Raphson method. The values of the parameters are as follows: $k_0 = 1\ \mu A/cm^2$, $K = 1.3 \times 10^{-6}$ L/mol, $r = 50$ kJ/mol, $g = 24$ kJ/mol. Comparison with experimental data (black circles in Figure 14) demonstrates that the proposed model can fit the data well with reasonable values of the parameters.[54,55] Thus, the rate-limiting step during CO oxidation in the prepeak region is concluded to be an L−H reaction involving Frumkin adsorption of OH at defect sites. It should be noted that a similar mechanism was previously proposed by Tripkovic et al. to describe methanol oxidation on Pt(111) in alkaline electrolytes,[29] where the Tafel slope and dependence on OH^- concentration (120 mV per decade and 0.55, respectively) were found to be very close to the values reported in this work for CO oxidation.

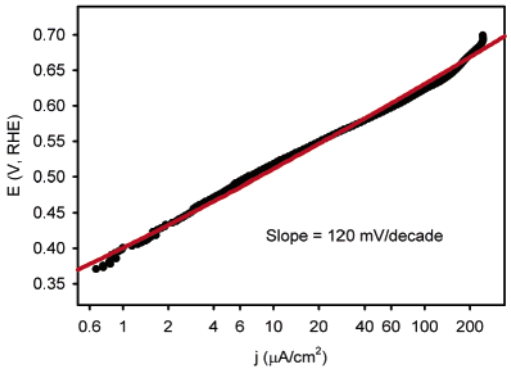

Figure 14. Bulk CO oxidation on well-ordered Pt(111) in 0.1 M NaOH. Black circles: experimental data collected at 2 mV/s. Red line: simulated data calculated from eqs 7 and 15 (see the text for the details of the calculation).

3.2.3. Effect of the Adsorption Environment. The local environment at the Pt(111) surface during CO adsorption influences the subsequent CO stripping voltammogram. Adsorption of CO in 0.1 M H_2SO_4, followed by rinsing with Ar/CO-saturated water and transfer to 0.1 M NaOH under an Ar blanket, produces a CO stripping voltammogram in which the prepeak is shifted to higher potential, to the extent that most of the CO that would typically be oxidized in the prepeak is now oxidized in the main peak (dashed trace in Figure 9). We have observed the same effect when performing the adsorption in 0.1 M $HClO_4$, in 0.05 mM $HClO_4$, and in the gas phase on a dry Pt(111) surface that was subsequently immersed in 0.1 M NaOH. Repeatedly oxidizing and re-forming a portion of the CO adlayer in a CO-saturated 0.1 M NaOH solution also produces the same effect. Notably, a similar shift of the prepeak to more positive potential occurs on lightly disordered Pt(111) surfaces, highly disordered Pt(111) surfaces, Pt(10 10 9) surfaces, and Pt(111)/Ru surfaces when CO is adsorbed in 0.1 M H_2SO_4. This phenomenon is difficult to explain if the mechanism of CO oxidation in the prepeak is E−R, since for the E−R mechanism the rate of CO oxidation at a given potential in 0.1 M NaOH should depend only on the CO binding energy and the fraction of CO−OH^- collisions that occur with the proper geometry for reaction. Neither of these should vary with the adsorption media, assuming that a similar CO adlayer is formed in each case, which seems probable on the basis of the similar CO adlayers observed under a variety of electrochemical conditions.[56] When only the case of well-ordered surfaces is examined, the role of the CO adlayer domain size may seem significant. According to Markovic et al.,[57] smaller (2×2)-3CO domains are formed

in alkaline solutions as compared with acid solutions (roughly 3 nm vs 14 nm). If similar domain size arguments also hold true for the lower coverage adlayer structures that form after removal of CO from solution,[58] then larger CO adlayer domains for adlayers formed in acidic solutions could be proposed as the cause of the shift in the prepeak, since CO molecules adsorbed at domain boundaries and other defects in the CO adlayer would likely be more labile for E−R oxidation than CO molecules within well-ordered CO domains. Although such an argument could possibly be made for well-ordered Pt(111), the argument breaks down on the more heterogeneous disordered and bimetallic surfaces, where the Pt(111) domains are similar in size to the (2×2)-3CO domains observed by Markovic et al., leading to CO domains that should be similar in size regardless of the pH of the solution in which CO was adsorbed. Therefore, the observation of a shift in the prepeak as a result of changes in the local environment during CO adsorption can be considered as more evidence against an E−R mechanism for CO oxidation in the prepeak. Such a shift can be readily explained by the availability of defects for adsorption of OH, the oxidant in the L−H mechanism. In alkaline solutions, some OH, or precursor to OH (water), is adsorbed even at low potentials, and this species cannot be completely removed from the defect sites by CO adsorption. This explanation is consistent with the observation of a high initial current during potentiostatic CO oxidation in the prepeak region. Therefore, the CO adlayer formed in alkaline solutions is already primed for oxidation by this low coverage of OH adsorbed at defects. Adlayers formed in acidic solutions lack this OH species at defect sites. In acid, such a suppression of adsorbed OH could be reasonably assigned to competition with other specifically adsorbing anions, present either as the conjugate base of the acid electrolyte (e.g., HSO_4^- in H_2SO_4 solutions) or as a contaminant (e.g., Cl^- in $HClO_4$ solutions[59]). For CO adlayers formed in the gas phase, exclusion of water from the surface would be expected to cause the suppression of OH adsorption. This interpretation is in agreement with the observation that, for CO/D_2O adlayers formed in a UHV, the order of adsorption affects the resulting adlayer structure.[60,61] While Pt(111)−D_2O surfaces exposed to CO form intermixed CO/D_2O adlayers, Pt(111)−CO-saturated adlayers exposed to D_2O do not incorporate any D_2O into the innermost adsorbate layer, instead adsorbing D_2O on top of the CO adlayer. Of course, the UHV studies had to be performed at temperatures of around 150 K, since water desorbs at higher temperatures in a UHV environment. At room temperature, which was used in the present study, the ability of CO to effectively exclude water from the innermost adsorbate layer is debatable. However, CO adlayers formed in the gas phase in this study had a higher coverage (about 0.65 ML) than those formed in the UHV studies (about 0.5 ML) due to a higher CO partial pressure of about 10 Torr during adlayer formation.[62] Since the ability of CO to exclude water from the innermost adsorbate layer increases with the CO coverage,[60,61] water could likely be excluded even at room temperature with the high CO coverage employed in the present study. The exclusion of water from the metal surface would prevent the formation of adsorbed OH, and thus inhibit L−H CO oxidation. In contrast, E−R CO oxidation should not be significantly affected by the formation of such an adlayer, so the results are again in better agreement with the L−H mechanism.

As described above, repeatedly oxidizing and readsorbing a fraction of the CO adlayer in CO-saturated 0.1 M NaOH solution can also suppress the prepeak. In this case, the OH at defect sites is consumed by reaction with CO, and the rate of OH readsorption at defect sites is apparently not fast enough to keep these defects from being covered by CO. Once covered, OH cannot readsorb until the blocking CO is removed. Thus, the results obtained by varying the adsorption procedure to suppress the prepeak, including adsorption in acidic solutions, adsorption from the gas phase, or adsorption in CO-saturated alkaline solutions in which the prepeak is repeatedly oxidized, are in better agreement with the proposed L−H mechanism of CO oxidation than the E−R mechanism.

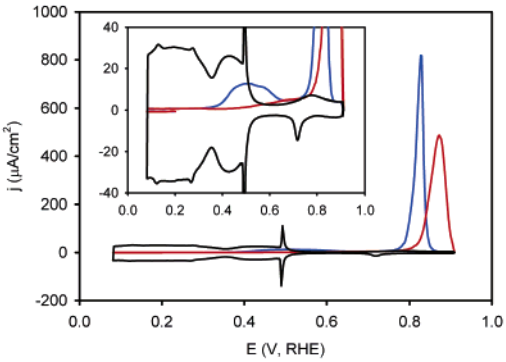

Figure 15. Effect of the adsorption environment on CO stripping in 0.1 M H_2SO_4. Red line: CO adsorbed at 0.10 V in 0.1 M H_2SO_4. Blue line: CO adsorbed at 0.10 V in 0.1 M NaOH, followed by rinsing with CO-saturated water and transfer to 0.1 M H_2SO_4 under an Ar blanket. Black line: background CV collected after stripping of CO adsorbed in 0.1 M NaOH.

Further evidence for the existence of reactive OH (or an OH precursor) adsorbed at defects on a CO-saturated Pt(111) surface at low potentials in alkaline media comes from stripping voltammograms, collected in acidic solutions, of a CO adlayer that was formed in 0.1 M NaOH. Voltammetric oxidation of a CO adlayer formed in an alkaline solution produces a prepeak that is much larger, and shifted to lower potential, than the prepeak in a similar stripping voltammogram for CO adsorbed in acid (Figure 15). The oxidation of CO in the prepeak for the typical case, in which CO is adsorbed and oxidized in acidic media, is known to occur because of the weak CO adsorption at the highest coverages, resulting in a more reactive adsorbed CO species which is oxidized by OH at defect sites.[63] Since this weakly adsorbed CO desorbs continuously after the removal of CO from solution, the size of the prepeak decreases with increasing Ar purge time. The prepeak shown in the dotted trace in Figure 15 is typical for CO adsorption followed by a 1−2 min Ar purge, while for a 10 min Ar purge the prepeak completely disappears. When the CO is adsorbed in alkaline media and transferred to acid, the unusually large prepeak shows a much weaker dependence on time than when the CO is adsorbed in acid, remaining quite large even after 10 min of exposure to CO-free solution. This behavior suggests that a weakened Pt−CO bond strength is not the only factor giving rise to the large prepeak at low potential when CO is adsorbed in alkaline media. Rather, we propose that a highly reactive OH species formed at defects in the case of alkaline-adsorbed CO is responsible for the large prepeak at unusually low potential. After oxidation of the prepeak, the remaining CO is oxidized in a peak that is sharper and at lower potential than normal for a well-ordered Pt(111) surface. The change in the main peak morphology for the CO adlayer formed in alkaline solution is due to the lower CO coverage remaining after oxidation of the unusually large prepeak. We note that a similar peak position and morphology is known to result in some cases from a high surface defect density,[64] but in the present case, the existence of extensive, well-ordered Pt(111) domains (as

indicated by the large "butterfly" peak) rules out a significant role of surface defects in causing the observed peak shift.

Having concluded that CO oxidation on Pt(111) in alkaline media occurs through an L−H mechanism, it is interesting to note that the simultaneous presence of adsorbed CO and OH is not sufficient to cause CO oxidation to occur, as illustrated in Figure 8. In the dashed trace of Figure 8, 0.17 ML of CO is present on the surface, yet the adsorption of OH at small islands occurs at 0.54 V without any significant oxidation of CO. For CO coverage lower than 0.20 ML, the CO oxidation reaction does not occur unless OH is adsorbed on terraces; there is no prepeak. At the highest CO coverage, CO can be oxidized at potentials as low as 0.25 V by OH adsorbed at defects. As the CO coverage decreases, the Pt−CO bond strength increases dramatically,[65,66] such that CO is no longer able to react with OH adsorbed at defects. In contrast, OH adsorbed on terraces is more weakly bound than OH on defects, and thus is able to react with CO even at very low CO coverage. The important conclusion is that simply providing adsorbed CO and OH is not enough for reaction to occur; the strength of adsorption is also a significant factor in determining reactivity.

4. Summary and Conclusions

On well-ordered Pt(111) surfaces, the unavoidable presence of a small number of defects results in a very small, but nonzero, coverage of OH at potentials less positive than the onset potential for OH adsorption on terraces. Scanning the potential up to 1.25 V produces small Pt islands (<1 nm diameter). The edges of the small islands are characterized by adsorption sites that have the same geometry as kinks. Scanning the potential to higher values results in the appearance of 1−4 nm Pt islands. The edges of these islands are characterized by adsorption sites with (110) and (100) geometry. Small islands show a well-defined OH adsorption peak at 0.49 V, while large islands adsorb a small coverage of OH even in the H adsorption region.

Defect-bound OH species are active for Langmuir−Hinshelwood CO oxidation at low potential on a CO-saturated surface, as demonstrated by the peaked current transient during potentiostatic CO oxidation, but at low CO coverage the Pt−CO bond is too strong for oxidation by OH at defects. Oxidation of this strongly bound CO requires reaction with OH adsorbed on terraces, where it is more weakly bound than on defects, and thus more reactive.

In the prepeak region (less positive than 0.7 V), where defect-bound OH is the oxidant, the high value of the measured Tafel slope (130 mV per decade) and the reaction order in OH^- (0.5) are compatible with a Langmuir−Hinshelwood rate-limiting reaction of CO with adsorbed OH, in which OH adsorption is described by the Frumkin isotherm. The high Tafel slope rules out oxidation of COOH as the rate-limiting step, while the subunity reaction order in OH^- rules out OH adsorption as the rate-limiting step. Similarly, the subunity reaction order in OH^- rules out the possibility of an Eley−Rideal rate-limiting step. Adsorption of the reactive OH at defects is not limited by CO (noncompetitive adsorption), except at the highest CO coverage, achieved only in the presence of CO dissolved in solution.

In the main peak region, the measured Tafel slope (73 mV per decade) is consistent with an oxidation reaction in which the rate-limiting step is the Langmuir−Hinshelwood reaction between CO and OH adsorbed on terraces. In this region, CO and OH compete for adsorption sites at all coverages, though the low CO coverage following oxidation of the prepeak makes the competition difficult to observe in most cases.

The nature of the adsorbed CO and coadsorbates such as OH and H_2O varies with the CO adsorption method. Some OH, or OH precursor (H_2O), is present at defects even at low potentials when CO is adsorbed in alkaline solutions, giving rise to a large prepeak when CO is subsequently oxidized in 0.1 M NaOH or 0.1 M H_2SO_4. In contrast, adsorption of CO in acidic solutions or in the gas phase prevents formation of this OH species, so that the prepeak is much smaller and shifted to higher potential when CO is subsequently oxidized in 0.1 M NaOH or 0.1 M H_2SO_4.

A good understanding of the CO oxidation mechanism on Pt surfaces is required for the rational design of electrocatalysts for fuel cells. The identification of a Langmuir−Hinshelwood mechanism for CO oxidation in both the prepeak and main peak regions in alkaline solutions is thus a significant step in the development of alkaline fuel cells. The inability of CO to react with defect-bound OH at low CO coverage has significant implications for methanol oxidation in alkaline media, since even a low CO coverage can completely inhibit methanol oxidation.[67] Therefore, future studies of CO oxidation in alkaline media should consider the role of CO and OH adsorption strength, since the results presented here show that the defect-bound OH species present at low potentials on lightly disordered Pt(111) surfaces is too strongly adsorbed to react with CO at low CO coverage.

Acknowledgment. This work is supported by the Army Research Office under DDD Grant DAAD19-03-1-0169 and by the DOE under Grant DE-FG02005ER46260. J.S.S. acknowledges support from a National Science Foundation Graduate Research Fellowship.

References and Notes

(1) Love, B.; Lipkowski, J. *ACS Symp. Ser.* **1988**, *378*, 484.
(2) Zurawski, D.; Wasberg, M.; Wieckowski, A. *J. Phys. Chem.* **1990**, *94*, 2076.
(3) Bergelin, M.; Herrero, E.; Feliu, J. M.; Wasberg, M. *J. Electroanal. Chem.* **1999**, *467*, 74.
(4) Herrero, E.; Alvarez, B.; Feliu, J. M.; Blais, S.; Radovic-Hrapovic, Z.; Jerkiewicz, G. *J. Electroanal. Chem.* **2004**, *567*, 139.
(5) Lebedeva, N. P.; Koper, M. T. M.; Feliu, J. M.; van Santen, R. A. *J. Electroanal. Chem.* **2002**, *524*, 242.
(6) Lopez-Cudero, A.; Cuesta, A.; Gutierrez, C. *J. Electroanal. Chem.* **2005**, *579*, 1.
(7) Batista, E. A.; Iwasita, T.; Vielstich, W. *J. Phys. Chem. B* **2004**, *108*, 14216.
(8) Petukhov, A. V.; Akemann, W.; Friedrich, K. A.; Stimming, U. *Surf. Sci.* **1998**, *404*, 182.
(9) Wieckowski, A.; Rubel, M.; Gutierrez, C. *J. Electroanal. Chem.* **1995**, *382*, 97.
(10) Schmidt, T. J.; Ross, P. N.; Markovic, N. M. *J. Phys. Chem. B* **2001**, *105*, 12082.
(11) Spendelow, J. S.; Lu, G. Q.; Kenis, P. J. K.; Wieckowski, A. *J. Electroanal. Chem.* **2004**, *568*, 215.
(12) Santos, E.; Giordano, M. C. *J. Electroanal. Chem.* **1984**, *172*, 201.
(13) Markovic, N. M.; Schmidt, T. J.; Grgur, B. N.; Gasteiger, H. A.; Behm, R. J.; Ross, P. N. *J. Phys. Chem. B* **1999**, *103*, 8568.
(14) Kita, H.; Shimazu, K.; Kunimatsu, K. *J. Electroanal. Chem.* **1988**, *241*, 163.
(15) Hachkar, M.; Napporn, T.; Leger, J. M.; Beden, B.; Lamy, C. *Electrochim. Acta* **1996**, *41*, 2721.
(16) McLean, G. F.; Niet, T.; Prince-Richard, S.; Djilali, N. *Int. J. Hydrogen Energy* **2002**, *27*, 507.
(17) Choban, E. R.; Markoski, L. J.; Wieckowski, A.; Kenis, P. J. A. *J. Power Sources* **2004**, *128*, 54.
(18) Choban, E. R.; Spendelow, J. S.; Gancs, L.; Wieckowski, A.; Kenis, P. J. A. *Electrochim. Acta* **2005**, *50*, 5390.
(19) Jayashree, R. S.; Gancs, L.; Choban, E. R.; Primak, A.; Natarajan, D.; Markoski, L. J.; Kenis, P. J. A. *J. Am. Chem. Soc.* **2005**, *127*, 16758.
(20) Cohen, J. L.; Westly, D. A.; Pechenik, A.; Abruna, H. D. *J. Power Sources* **2005**, *139*, 96.
(21) Jayashree, R. S.; Egas, D.; Spendelow, J. S.; Natarajan, D.; Markoski, L. J.; Kenis, P. J. A. *Electrochem. Solid State Lett.*, in press.
(22) Baxter, R. J.; Hu, P. *J. Chem. Phys.* **2002**, *116*, 4379.
(23) Sun, S. G.; Chen, A. C. *J. Electroanal. Chem.* **1992**, *323*, 319.

(24) Clavilier, J.; Albalat, R.; Gomez, R.; Orts, J. M.; Feliu, J. M.; Aldaz, A. *J. Electroanal. Chem.* **1992**, *330*, 489.
(25) Hernandez-Ferrer, J.; Herrero, E.; Feliu, J. M.; Clavilier, J. *Abstracts of the 203rd ECS Meeting*; Electrochemical Society: Pennington, NJ, 2003; Abstract 1251.
(26) Fiedler, J.; Salmain, M.; Jaouen, G.; Pospisil, L. *Inorg. Chem. Commun.* **2001**, *4*, 613.
(27) Wagner, F. T.; Ross, P. N. *J. Electroanal. Chem.* **1988**, *250*, 301.
(28) Marinkovic, N. S.; Markovic, N. M.; Adzic, R. R. *J. Electroanal. Chem.* **1992**, *330*, 433.
(29) Tripkovic, A. V.; Popovic, K. D.; Momcilovic, J. D.; Drazic, D. M. *J. Electroanal. Chem.* **1996**, *418*, 9.
(30) Lebedeva, N. P.; Koper, M. T. M.; Feliu, J. M.; van Santen, R. A. *J. Phys. Chem. B* **2002**, *106*, 12938.
(31) Kobayashi, T.; Babu, P. K.; Gancs, L.; Chung, J. H.; Oldfield, E.; Wieckowski, A. *J. Am. Chem. Soc.* **2005**, *127*, 14164.
(32) Cai, Y.; Anderson, A. B. *J. Phys. Chem. B* **2005**, *109*, 7557.
(33) Teliska, A.; O'Grady, W. E.; Ramaker, D. E. *J. Phys. Chem. B* **2005**, *109*, 8076.
(34) Burke, L. D.; Collins, J. A.; Horgan, M. A.; Hurley, L. M.; O'Mullane, A. P. *Electrochim. Acta* **2000**, *45*, 4127.
(35) Climent, V.; Gomez, R.; Orts, J. M.; Rodes, A.; Aldaz, A.; Feliu, J. M. Electrochemistry, Spectroscopy, and Scanning Tunneling Microscopy Images of Small Single-Crystal Electrodes. In *Interfacial Electrochemistry: Theory, Experiment, and Applications*; Wieckowski, A., Ed.; Marcel Dekker: New York, 1999; p 463.
(36) Spendelow, J. S.; Goodpaster, J. D.; Kenis, P. J. A.; Wieckowski, A. Manuscript in preparation.
(37) Feibelman, P. J.; Esch, S.; Michely, T. *Phys. Rev. Lett.* **1996**, *77*, 2257.
(38) Wang, H.; Tobin, R. G.; Lambert, D. K.; DiMaggio, C. L.; Fisher, G. B. *Surf. Sci.* **1997**, *372*, 267.
(39) Sljivancanin, Z.; Hammer, B. *Surf. Sci.* **2002**, *515*, 235.
(40) McClellan, M. R.; McFeely, F. R.; Gland, J. L. *Surf. Sci.* **1983**, *124*, 188.
(41) Szabo, A.; Henderson, M. A.; Yates, J. T. *J. Chem. Phys.* **1992**, *96*, 6191.
(42) Morallon, E.; Vazquez, J. L.; Aldaz, A. *J. Electroanal. Chem.* **1990**, *288*, 217.
(43) Morin, M. C.; Lamy, C.; Leger, J. M.; Vasquez, J. L.; Aldaz, A. *J. Electroanal. Chem.* **1990**, *283*, 287.
(44) Rodes, A.; Clavilier, J. *J. Electroanal. Chem.* **1993**, *344*, 269.
(45) Herrero, E.; Orts, J. M.; Aldaz, A.; Feliu, J. M. *Surf. Sci.* **1999**, *440*, 259.
(46) Nieskens, D. L. S.; Ferre, D. C.; Niemantsverdriet, J. W. *ChemPhysChem* **2005**, *6*, 1293.
(47) Zurawski, D.; Chan, K.; Wieckowski, A. *J. Electroanal. Chem.* **1987**, *230*, 205.
(48) Ciobica, I. M.; Kleyn, A. W.; Van Santen, R. A. *J. Phys. Chem. B* **2003**, *107*, 164.
(49) McCallum, C.; Pletcher, D. *J. Electroanal. Chem.* **1976**, *70*, 277.
(50) Palaikis, L.; Zurawski, D.; Hourani, M.; Wieckowski, A. *Surf. Sci.* **1988**, *199*, 183.
(51) Santos, E.; Leiva, E. P. M.; Vielstich, W. *Electrochim. Acta* **1991**, *36*, 555.
(52) Bard, A. J.; Faulkner, L. R. *Electrochemical Methods*, 2nd ed.; Wiley: New York, 2001.
(53) Drazic, D. M.; Tripkovic, A. V.; Popovic, K. D.; Lovic, J. D. *J. Electroanal. Chem.* **1999**, *466*, 155.
(54) Obradovic, M. D.; Grgur, B. N.; Vracar, L. M. *J. Electroanal. Chem.* **2003**, *548*, 69.
(55) Jovic, B. M.; Jovic, V. D.; Stafford, G. R. *Electrochem. Commun.* **1999**, *1*, 247.
(56) Chang, S. C.; Jiang, X.; Roth, J. D.; Weaver, M. J. *J. Phys. Chem.* **1991**, *95*, 5378.
(57) Markovic, N. M.; Lucas, C. A.; Rodes, A.; Stamenkovi, V.; Ross, P. N. *Surf. Sci.* **2002**, *499*, L149.
(58) Rodes, A.; Gomez, R.; Feliu, J. M.; Weaver, M. J. *Langmuir* **2000**, *16*, 811.
(59) Arenz, M.; Stamenkovic, V.; Schmidt, T. J.; Wandelt, K.; Ross, P. N.; Markovic, N. M. *Surf. Sci.* **2003**, *523*, 199.
(60) Kizhakevariam, N.; Jiang, X. D.; Weaver, M. J. *J. Chem. Phys.* **1994**, *100*, 6750.
(61) Kinne, M.; Fuhrmann, T.; Zhu, J. F.; Trankenschuh, B.; Denecke, R.; Steinruck, H. P. *Langmuir* **2004**, *20*, 1819.
(62) Longwitz, S. R.; Schnadt, J.; Vestergaard, E. K.; Vang, R. T.; Laegsgaard, E.; Stensgaard, I.; Brune, H.; Besenbacher, F. *J. Phys. Chem. B* **2004**, *108*, 14497.
(63) Markovic, N. M.; Grgur, B. N.; Lucas, C. A.; Ross, P. N. *J. Phys. Chem. B* **1999**, *103*, 487.
(64) Lebedeva, N. P.; Koper, M. T. M.; Feliu, J. M.; van Santen, R. A. *Electrochem. Commun.* **2000**, *2*, 487.
(65) Ertl, G.; Neumann, M.; Streit, K. M. *Surf. Sci.* **1977**, *64*, 393.
(66) Yeo, Y. Y.; Vattuone, L.; King, D. A. *J. Chem. Phys.* **1997**, *106*, 392.
(67) Spendelow, J. S.; Goodpaster, J. D.; Johnston, C. M.; Kenis, P. J. A.; Wieckowski, A. Manuscript in preparation.